Available online at www.sciencedirect.com
ScienceDirect
Journal of Catalysis 255 (2008) 197–205
JOURNAL OF CATALYSIS
www.elsevier.com/locate/jcat

CH_3OH oxidation over well-defined supported V_2O_5/Al_2O_3 catalysts: Influence of vanadium oxide loading and surface vanadium–oxygen functionalities

Taejin Kim, Israel E. Wachs *

Operando Molecular Spectroscopy and Catalysis Laboratory, Chemical Engineering Department, Lehigh University, Bethlehem, PA 18015, USA

Received 21 May 2007; revised 4 February 2008; accepted 6 February 2008

Available online 14 March 2008

Abstract

A series of supported V_2O_5/Al_2O_3 catalysts were synthesized by incipient wetness impregnation with vanadium isopropoxide in isopropanol solutions and subsequent calcination. The vanadium surface density was varied from 0.3 to 11.4 V atoms/nm^2 spanning the sub-monolayer and above-monolayer regions. The resulting supported vanadium oxide catalysts were physically characterized with *in situ* Raman spectroscopy and chemically probed by CH_3OH TPSR and steady-state methanol oxidation. The Raman characterization under dehydrated conditions revealed that the supported vanadium oxide catalysts contained only surface vanadia species below monolayer coverage (100% dispersed) and both surface vanadia species and crystalline V_2O_5 nanoparticles (NPs) above monolayer coverage. The CH_3OH oxidative dehydrogenation kinetic parameters were found to be independent of the surface bridging V–O–V bond concentration (polymerization extent), surface V=O bond length/strength, vanadium surface density on the alumina support, surface acidity, and surface vanadia reduction characteristics during H_2-TPR. The crystalline V_2O_5 NPs above monolayer coverage were relatively inactive and served only to decrease the number of exposed catalytic active surface vanadia sites by covering them.

Keywords: Spectroscopy; Raman; TPSR; Catalysts; Supported; V_2O_5; Al_2O_3; Reaction; Oxidation; CH_3OH; HCHO

1. Introduction

Supported vanadium oxide catalysts consist of a two-dimensional surface vanadium oxide overlayer on high-surface area oxide supports (e.g., Al_2O_3, ZrO_2, TiO_2) and have received much attention in the catalysis literature because of their extensive industrial applications, such as methanol oxidation and reduction of NO_x emissions [1–10]. The presence of isolated and polymeric surface VO_4 species on the oxide supports in dehydrated supported vanadia catalysts was demonstrated by multiple characterization investigations: Raman spectroscopy [11–18], X-ray absorption spectroscopy (EXAFS and XANES) [19,20], solid-state ^{51}V NMR spectroscopy [21], FT-IR spectroscopy [14,22–24], X-ray photoelectron spectroscopy (XPS) [25–28], and UV–vis diffuse reflection spectroscopy (DRS) [29–31]. More recently, supported vanadium oxide catalysts also have received fundamental attention as model-supported metal oxide catalyst systems.

The oxidative dehydrogenation of CH_3OH to HCHO over supported vanadium oxide as well as vanadium-containing heteropolyoxo anion (HPA) catalysts has received much attention in the catalysis literature. Sorenson and Weber found that the reaction rate for CH_3OH oxidation to HCHO increases linearly with number of vanadium atoms ($n = 1$, 2 or 3) present in the $[PW_{12-n}V_nO_{40}]^{(3+n)-}$ HPAs, which translates to a constant TOF when normalized per vanadium content [7]. The constant TOF with increasing vanadia sites in the HPA Keggin unit reveals that the oxidative dehydrogenation of methanol to formaldehyde involves only a single vanadium site. Deo and Wachs similarly found that the TOF for methanol oxidation over supported vanadium oxide catalysts is constant with vanadium content in the sub-monolayer region and also concluded

* Corresponding author. Fax: +1 610 758 6555.
E-mail address: iew0@lehigh.edu (I.E. Wachs).

0021-9517/$ – see front matter
doi:10.1016/j.jcat.2008.02.007

that this selective oxidation reaction involves only one surface VO_4 site [8].

The oxidation of CH_3OH over supported vanadium oxide catalysts is known to proceed via dissociative chemisorption to form surface V–OCH_3 and support–OH intermediates [31,32]. *In situ* IR analysis of the surface $CH_3O^{\cdot}$ species also has revealed that the surface methoxy is coordinated only to one vanadium site [32]. The rate-determining step (RDS) for the methanol oxidation reaction is the decomposition of the surface methoxy intermediate to form HCHO [33,34]. Recent density function theory (DFT) calculations suggest that CH_3OH adsorption occurs at the bridging V–O–support bond by forming the V–OCH_3 and support–OH intermediates [2,35,36]. The RDS involving surface methoxy C–H scission was proposed to occur by transfer of a methyl H atom to the V=O bond, with concurrent splitting of the V–OCH_2 bond to form the gaseous HCHO reaction product [2,36]. Earlier extended Huckel calculations proposed that the H atom initially may transfer as a hydride to the V atom, not its oxygen ligands, and involves only 1 VO_x site [37]. Extended Huckel calculations, however, provide not explicit information about barriers and pre-exponential factors that allow decisions between competitive mechanisms that are provided by DFT calculations.

The objectives of this paper are to address the following fundamental issues about CH_3OH oxidation to HCHO over model supported V_2O_5/Al_2O_3 catalysts:

- Contribution of the different V=O, V–O–V, and V–O–support oxygen functionalities.
- Relative oxidative catalytic activity of surface VO_4 monomers, surface VO_4 polymers and V_2O_5 nanoparticles (NPs).
- Determination of the kinetic parameters K_{ads}, k_{rds} and TOF.

In the present work, these basic issues will be addressed by (i) varying the relative concentration of isolated VO_4 species, polymeric surface VO_4 species and crystalline V_2O_5 NPs on Al_2O_3; (ii) probing the surface chemistry with CH_3OH temperature-programmed surface reaction (TPSR) spectroscopy; and (iii) and performing steady-state CH_3OH oxidation to H_2CO. Combination of the TPSR and steady-state methanol oxidation studies allows for quantitative determination of the kinetic parameters (TOF, K_{ads} and k_{rds}) for the oxidative dehydrogenation of CH_3OH to HCHO and H_2O by the supported V_2O_5/Al_2O_3 catalysts.

2. Experimental

2.1. Catalyst synthesis

The Al_2O_3 support (Engelhard, $S_{BET} = 215\ m^2/g$) used in this study was calcined in air at 450–500 °C and cooled to room temperature before being impregnated with the vanadium oxide precursor. The supported V_2O_5/Al_2O_3 catalysts were prepared by incipient wetness impregnation of a 2-propanol solution of vanadium isopropoxide [$VO(O\text{-}Pr^i)_3$; Alfa-Aesar, 97% purity] onto the Al_2O_3 support. The preparation was performed inside a glove box with continuously flowing N_2 because of the moisture sensitivity of the precursor. After impregnation, the samples were kept inside the glove box to dry overnight. The samples were then further dried in flowing N_2 at 120 °C for 1 h and 300 °C for 1 h, and finally calcined in flowing air at 300 °C for 1 h and 450 °C for 2 h.

2.2. BET specific surface area

The BET surface areas of the samples were determined by N_2 adsorption–desorption at −196 °C using a Quantachrome Quantasorb OS-9 surface area analyzer. A sample quantity of 30 mg was used, and the sample was outgassed at 250 °C before N_2 adsorption using a Quantachrome QT-3 device. The surface density of the supported vanadia phase on the oxide supports is expressed as V atoms/nm^2.

2.3. Raman spectroscopy

The *in situ* Raman spectra of the dehydrated supported vanadium oxide catalysts were collected with a Horiba-Jobin Yvon LabRam-HR spectrophotometer equipped with a confocal microscope (Olympus BX-30), notch filter (532 nm), and a 900-grooves/mm grating. The catalysts were excited with 532 nm excitation (Coherent 315 m Yag double-diode pumped laser, 20 mW) in the 200–1200 cm^{-1} region. The spectral resolution was ∼1 cm^{-1}. The scattered photons were directed into a single-stage monochromator and focused onto a LN_2-cooled CCD detector (JY-CCD3000V). The Raman spectrometer was equipped with an *in situ* environmental cell (Linkam T1500) in which both the temperature and the gaseous composition were controllable. The Raman spectra of the dehydrated samples were collected at room temperature after heating at 450 °C for 1 h in flowing 10% O_2/argon (Airgas, ultra-high purity and hydrocarbon-free). A spectral acquisition time of 30 s/scan was used, for a total of 15 min/spectrum.

2.4. CH_3OH temperature-programmed surface reaction (TPSR) spectroscopy

The surface chemistry and reactivity of the supported vanadium oxide catalysts were chemically probed by CH_3OH TPSR spectroscopy, using an Altamira AMI-200 spectroscope equipped with a Dycor Dymaxion DME200MS online quadrupole mass spectrometer. In the presence of surface redox sites such as surface vanadia sites, CH_3OH oxidizes primarily to yield formaldehyde (HCHO). The catalysts were pretreated at 400 °C in flowing 10% O_2/He (Airgas, ultra-zero grade air, 30 mL/min) for 40 min to remove moisture and any possible oxidizable surface residues. Then the catalysts were cooled in the oxidizing environment to 110 °C, then switched to flowing He (Airgas, ultra-high purity, 30 mL/min) and further cooled to 100 °C. The methanol was chemisorbed at 100 °C from a CH_3OH/He flowing mixture (Airgas, 2000 ppm CH_3OH, 30 mL/min) for 30 min. Previous work demonstrated that methanol adsorption at 100 °C minimizes the formation of

physically adsorbed methanol on the samples, because physically adsorbed CH_3OH desorbs below this temperature from oxide surfaces [40]. After allowing for adsorption of CH_3OH on the catalysts, the samples were purged for 1 h in flowing He to remove any residual physically adsorbed methanol, and the sample temperature was then increased in the flowing He at a rate of 10 °C/min. The reaction products desorbing from the catalysts were monitored by online mass spectrometry (MS). The m/e values of CH_3OH ($m/e = 31$), HCHO ($m/e = 30$), and CH_3OCH_3 ($m/e = 45$) were monitored to detect the different desorption products.

The decomposition kinetics of the surface $CH_3O^{\cdot}$ intermediate to HCHO and $H^{\cdot}$ occurs on surface vanadia redox sites and is known to follow a first-order reaction with a pre-exponential factor of $\sim 10^{13}$ s^{-1} [41]. The activation energy, E_a, for HCHO formation from the decomposition of the surface $CH_3O^{\cdot}$ intermediate was calculated from the Redhead equation [41,42],

$$\frac{E_a}{RT_p^2} = \frac{\nu}{\beta} \exp\left(-\frac{E_a}{RT_p}\right), \tag{1}$$

where T_p represents the TPSR peak temperature, $\nu = 10^{13}$ s^{-1} for first-order kinetics, β is the heating rate (10 °C/min), and R is the gas constant. The first-order rate constant, k_{rds}, for surface $CH_3O^{\cdot}$ was determined at the reference temperature of 230 °C with the Arrhenius equation,

$$k_{rds} = \nu \exp(-E_a/RT). \tag{2}$$

The number of exposed catalytic active sites per square meter, N_s, also was determined from the area under the H_2CO/CH_3OH TPSR curves and referenced to the N_s value of monolayer surface vanadia catalysts (8 V/nm^2). Below monolayer coverage, N_s was simply taken to be the number of vanadium atoms in the catalyst. Above monolayer coverage, N_s was determined from CH_3OH TPSR.

Minor amounts of reaction-limited CH_3OH and CH_3OCH_3 (DME) also were formed during the CH_3OH TPSR spectroscopy experiments. But DME was a significant product from the exposed acidic alumina sites at low surface vanadia coverage [43]. The reaction-limited CH_3OH arises from the reversible reaction of surface $CH_3O^{\cdot}$ and $H^{\cdot}$ [40,41]. The TPSR spectra for CH_3OH and DME formation are not presented in this paper, because the focus of the present study was on the redox properties of the surface vanadia species. Production of CO/CO_2 also is not discussed, because these products arise from readsorption of HCHO and are secondary oxidation reactions.

2.5. Steady-state methanol oxidation

Steady-state methanol oxidation was used to chemically probe the catalytic activity and selectivity of the supported vanadium oxide catalysts. The oxidation of methanol was examined in a fixed-bed reactor at 230 °C with ~30 mg of catalyst. The catalysts were suspended between two layers of quartz wool in a vertical glass tube. The volume composition of the gaseous reactant feed was $CH_3OH/O_2/He = 6/13/81$ (mol%), with a total flow rate of 100 mL/min, and the flow was from the top to the bottom of the reactor. The outlet line of the reactor to the gas chromatograph was heated to ~130 °C to avoid product condensation. Online analysis of methanol conversion and reaction products was performed with an HP-5840A gas chromatograph containing 2 packed columns (Porapack R and Carbosieve SII) and 2 detectors (TCD and FID). The supported vanadium oxide catalysts were pretreated at 350 °C for 1 h in flowing O_2/He before each run, after which the catalyst bed was cooled to 230 °C to initiate the reaction. The steady-state methanol oxidation catalytic data are expressed in terms of turnover frequency (TOF; number of HCHO molecules formed per surface vanadia site per s). The supported vanadia phases were 100% dispersed on the oxide supports below monolayer coverage, as shown below; for below-monolayer coverage, the number of catalytic active sites (N_s) was taken as the total number of supported vanadia atoms in the catalyst. Above monolayer coverage, the crystalline V_2O_5 NPs resided on top of the surface VO_x monolayers, and the number of exposed catalytic active sites was determined from the areas under the $HCHO/CH_3OH$ TPSR spectral curves by referencing against the monolayer supported vanadium oxide catalysts.

Table 1
BET surface area and vanadium surface density (V/nm^2) of the supported vanadium oxide catalysts

Sample	Surface areas (m^2/g)	Surface density (V/nm^2)
Bulk Al_2O_3	215	0
1 wt% V_2O_5/Al_2O_3	210	0.3
2 wt% V_2O_5/Al_2O_3	205	0.6
3 wt% V_2O_5/Al_2O_3	205	0.9
4 wt% V_2O_5/Al_2O_3	204	1.3
5 wt% V_2O_5/Al_2O_3	197	1.6
6 wt% V_2O_5/Al_2O_3	196	2.0
10 wt% V_2O_5/Al_2O_3	193	3.4
15 wt% V_2O_5/Al_2O_3	173	5.7
20 wt% V_2O_5/Al_2O_3	168	7.9
27 wt% V_2O_5/Al_2O_3	157	11.4

3. Results

3.1. BET specific surface area and vanadium oxide surface density

The resulting BET surface area and vanadium oxide surface density for the synthesized supported V_2O_5/Al_2O_3 catalysts of this study and are given in Table 1. The surface areas of the supported vanadia catalysts continually decreased with increasing vanadium oxide loading, due primarily to the added mass of the supported vanadia phase and also to minor losses in surface areas of the oxide supports during calcination. The vanadium surface density (V/nm^2) was determined by normalizing against the final surface area of the oxide supports after correcting for the mass contribution of the vanadium oxide component.

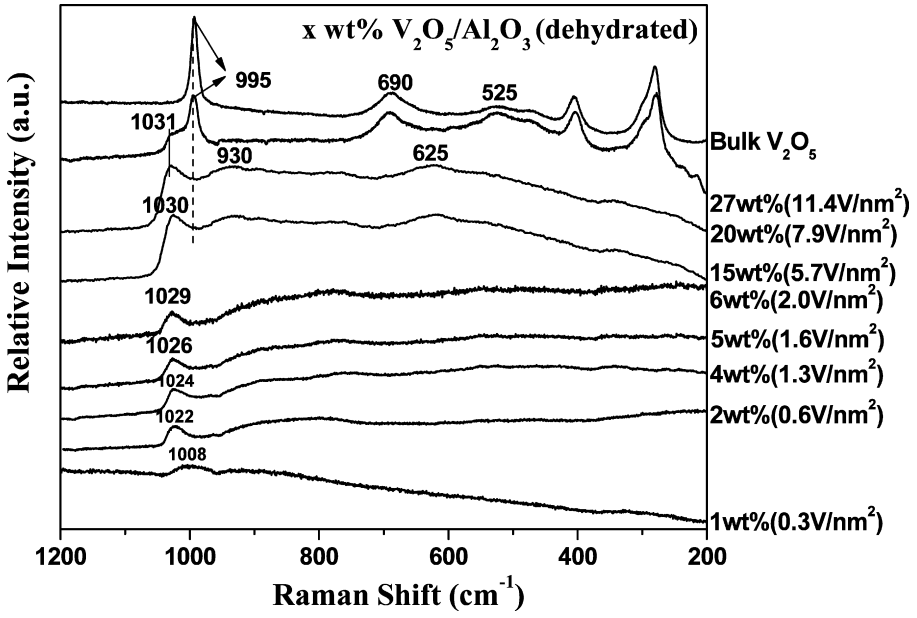

Fig. 1. *In situ* Raman spectra of supported V_2O_5/Al_2O_3 catalysts under dehydrated conditions.

3.2. In situ Raman spectroscopy

The *in situ* Raman spectra of the dehydrated supported V_2O_5/Al_2O_3 catalysts as a function of vanadium oxide loading, 0.3–11.4 V/nm^2, are shown in Fig. 1. The high-surface area Al_2O_3 support did not give rise to any Raman bands, allowing examination of vanadium oxide vibrations in the supported V_2O_5/Al_2O_3 catalysts. The Raman spectrum of the 1% V_2O_5/Al_2O_3 (0.3 V/nm^2) sample exhibited a broad band at ∼1008 cm^{-1} arising from the terminal V=O vibration of the surface VO_4 species [13,44–48]. The terminal V=O Raman band shifted from 1008 to 1031 cm^{-1} with increasing surface vanadia coverage. This shift in the surface V=O band with increasing vanadium oxide surface density is related to distortions associated with polymerization of the surface VO_4 species with increasing surface vanadia coverage [49]. The presence of bridging V–O–V bonds at high surface vanadium oxide coverage is reflected by the ∼625 cm^{-1} band [50]. At high surface vanadia loadings, the bridging V–O–Al vibration at 930 cm^{-1} also became more pronounced [36]. Crystalline V_2O_5 NPs (Raman bands at 995, 690, and 525 cm^{-1}) were not present up to 20% V_2O_5/Al_2O_3 (7.9 V/nm^2) catalyst sample and were present only at higher vanadium oxide surface densities. The appearance of crystalline V_2O_5 at higher vanadium surface density reflects completion of the surface vanadia monolayer on the Al_2O_3 support at ∼8 V/nm^2.

3.3. CH_3OH TPSR spectroscopy

The surface chemistry and number of exposed vanadia sites were chemically probed by CH_3OH TPSR spectroscopy. For the redox surface vanadia sites, CH_3OH dissociatively chemisorbed as surface $CH_3O^{\bullet}$ and $H^{\bullet}$, and the TPSR spectrum reflects the kinetics of breaking the C–H bond of the surface $CH_3O^{\bullet}$ intermediate (the RDS) to yield HCHO and surface $H^{\bullet}$. The kinetics of this step is reflected by the peak maximum (T_p), and the areas under the curves are proportional to the number of exposed catalytic active sites (N_s). The surface $H^{\bullet}$ subsequently reacts with surface $O^{\bullet}$ to from H_2O vapor. The TPSR experiments were performed in flowing He, because this reaction on the supported vanadium oxide catalysts proceeds by the Mars–van Krevelen mechanism, which requires oxygen only from the surface vanadia phase [51].

The main CH_3OH TPSR reaction product from the supported V_2O_5/Al_2O_3 catalysts was HCHO, with DME forming only at low vanadium oxide surface densities where exposed acidic Al_2O_3 sites were present. DME formation rapidly decreased with increasing vanadia coverage and was completely suppressed as monolayer surface vanadia coverage (∼8 V/nm^2) was approached (spectra not shown for brevity). As mentioned in the Experimental section, formation of CO and CO_2 resulted from readsorption of H_2CO; we do not discuss these secondary oxidation reactions in this paper. Furthermore, CO and CO_2 have not been found as reaction products in steady-state studies at low methanol conversions (see Section 3.4). The HCHO/CH_3OH TPSR spectra from the supported V_2O_5/Al_2O_3 catalysts, shown in Fig. 2, exhibited a constant T_p value of ∼191 °C as a function of vanadia content in the submonolayer region (0.9–7.9 V/nm^2). The presence of crystalline V_2O_5 NPs above monolayer coverage significantly decreased N_s, but did not change the T_p values (not shown for brevity). Thus, the catalytic active sites were the surface VO_4 species, and the crystalline V_2O_5 NPs did not appear to contribute to the overall catalytic activity, but served only to decrease the number of exposed surface VO_4 species.

The first-order rate constants for the breaking the C–H bond of surface $CH_3O^{\bullet}$ over the supported V_2O_5/Al_2O_3 catalysts were determined by application of the first-order Redhead equation [see Eqs. (1) and (2)] to the HCHO/CH_3OH TPSR spectra. The constant T_p value of ∼191 °C corresponds to a k_{rds} value of

0.164 s^{-1} and an E_a of 31.7 kcal/mol at the reference temperature of 230 °C, indicating that k_{rds} was independent of vanadium surface density.

The number of exposed catalytic active redox sites (N_s) for the supported V_2O_5/Al_2O_3 catalysts is plotted in Fig. 3 as a function of vanadium surface density. In the sub-monolayer region (<8 V/nm^2), the supported vanadia phase was 100% dispersed and the N_s values increased linearly with increasing vanadium surface density. Above monolayer coverage (>8 V/nm^2), the N_s values decreased with increasing vanadium surface density, because the relatively inert crystalline V_2O_5 NPs particles covered the catalytically active surface VO_4 species.

3.4. Steady-state methanol oxidation

The steady-state catalytic activity, TOF_{REDOX}, and selectivity performance of the supported V_2O_5/Al_2O_3 catalysts for methanol oxidation are given in Table 2. As for the CH_3OH TPSR experiments, the acidic surface Al_2O_3 sites led to the formation of DME, which rapidly decreased with increasing vanadia surface density, especially above monolayer coverage. The TOF_{REDOX} remained relatively constant for all vanadia surface densities (in both the sub-monolayer and above-monolayer regions), varying from 5 to 9 × 10^{-3} s^{-1} at 230 °C. The relatively constant TOF values above monolayer surface vanadium oxide coverage demonstrate that the primary effect of the crystalline V_2O_5 NPs was to just cover up the catalytic active surface VO_4 sites, because the crystalline V_2O_5 phase did not contribute significantly to the catalytic activity.

The methanol oxidation kinetics follows first-order dependence on CH_3OH partial pressure and zero-order dependence on oxygen partial pressure for supported vanadium oxide catalysts [2,56,58],

$$TOF = k_{rds}\, K_{ads}\, P_{CH_3OH}. \quad (3)$$

Earlier *in situ* IR studies revealed that the surface concentrations of the surface $CH_3O^{\cdot}$ intermediates are low under reaction conditions [38,39]. The kinetics of the surface RDS, k_{rds}, involves the breaking of the C–H bond of the surface $CH_3O^{\cdot}$ intermediate to form HCHO. The steady-state methanol oxidation kinetics provides the corresponding TOF values, and the value of P_{CH_3OH} is set by the experimental conditions. Consequently, the only remaining unknown kinetic parameter is K_{ads}

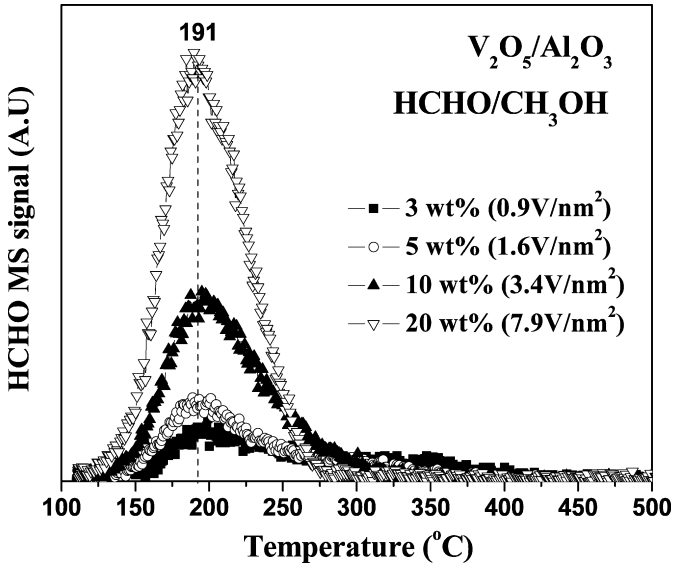

Fig. 2. HCHO/CH_3OH TPSR spectra from supported V_2O_5/Al_2O_3 catalysts as a function of vanadium oxide surface density (V/nm^2) in the sub-monolayer region.

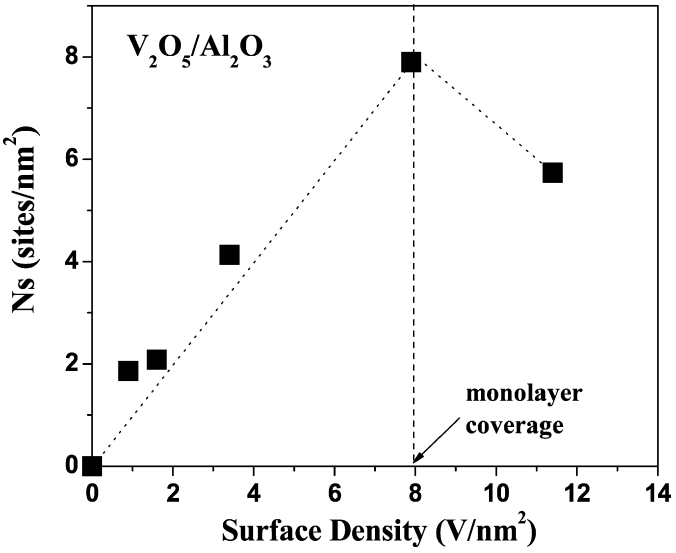

Fig. 3. Number of exposed sites/nm^2 for supported V_2O_5/Al_2O_3 catalysts as a function of vanadium surface density (V/nm^2).

Table 2
The kinetic values for methanol oxidation over supported vanadia catalysts as a function of vanadium surface density at 230 °C

Sample	SD (V/nm^2)	V–O–V polymeric concent. (%)[a]	V=O Raman band (cm^{-1})	E_a (kcal/mol)	k_{rds} (s^{-1})	K_{ads} (L/mol)	TOF_{REDOX} ×10^2 (s^{-1})	Selectivity (%)	
								Redox[b]	Acidic[c]
1 wt% V_2O_5/Al_2O_3	0.3	0.0	1008	31.7	0.164	19	0.45	1	99
3 wt% V_2O_5/Al_2O_3	0.9	0.0	1023	31.7	0.164	23	0.55	4	96
10 wt% V_2O_5/Al_2O_3	3.4	50.0	1029	31.7	0.164	31	0.74	14	86
15 wt% V_2O_5/Al_2O_3	5.7	84.0	1030	31.7	0.164	35	0.83	20	80
20 wt% V_2O_5/Al_2O_3	7.9	100.0	1031	31.7	0.164	27	0.64	50	50
27 wt% V_2O_5/Al_2O_3	11.4	100.0	1031	31.7	0.164	23	0.55	95	5

[a] From Ref. [49].
[b] HCHO, DMM and methyl formate.
[c] DME.

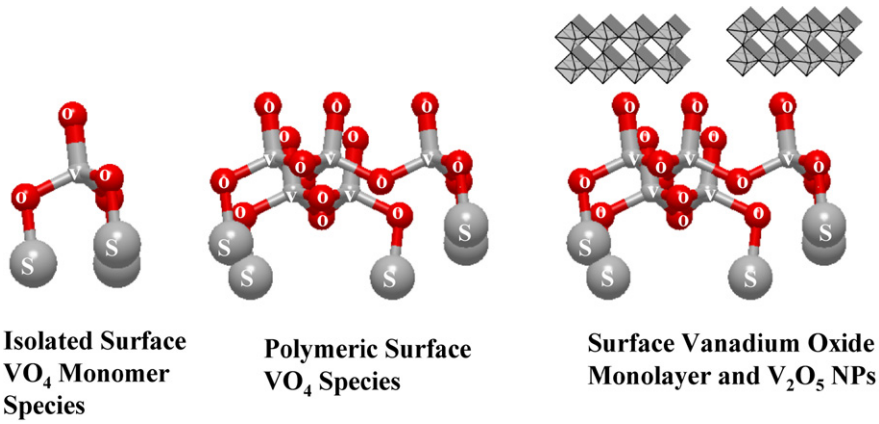

Fig. 4. Proposed molecular structures for supported vanadium oxide phase present for dehydrated supported vanadium oxide catalysts as a function of vanadium surface density.

that can be determined by rearranging Eq. (3) as

$$K_{ads} = \frac{TOF}{k_{rds}\, P_{CH_3OH}}. \quad (4)$$

Thus, combining the TPSR and steady-state methanol oxidation results allows us to determine the CH_3OH equilibrium adsorption constants for the supported vanadium oxide catalysts. The resulting K_{ads} values, presented in Table 2, varied slightly from 19 to 35 L/mol as a function of vanadium surface density at 230 °C. The relatively constant TOF and k_{rds} value for a given supported vanadium oxide catalyst system with coverage ensures that the K_{ads} values also will be relatively independent of vanadium surface density as a function of vanadium surface density. The slight variations in TOF and K_{ads}, within a factor of 2, are most likely related to experimental error.

4. Discussion

The dehydrated supported vanadium oxide catalysts consist of 2-dimensional surface VO_4 species in the sub-monolayer region (<8 V/nm^2). Crystalline V_2O_5 NPs are also present above monolayer coverage (>8 V/nm^2). The transition from the sub-monolayer region to the above-monolayer region (i.e., monolayer coverage) is reflected in the appearance of crystalline V_2O_5 NPs above monolayer surface coverage in the Raman spectra (see Fig. 1) and also to the decreased number of exposed vanadia sites with increasing vanadia surface density above monolayer (see Fig. 3). The decreased N_s values above monolayer coverage arose because of the platelet morphology of the V_2O_5 NPs that chemisorbed CH_3OH only at the edge planes and not the basal planes, which constitute most of the exposed vanadia sites [57,59,60]. Consequently, the presence of the crystalline V_2O_5 NPs had the primary effect of decreasing N_s by covering catalytic active surface VO_4 sites. Vohs et al. similarly found, from combined TGA-TPS studies of supported V_2O_5/TiO_2 catalysts, that the number of chemisorbed CH_3OH molecules decreased with increasing V_2O_5 NPs content above monolayer surface vanadium oxide coverage [41]. The molecular structure of the dehydrated supported vanadium oxide phase with vanadium surface density is schematically depicted in Fig. 4.

In situ UV–vis DRS has demonstrated that the surface VO_4 species present in the dehydrated supported V_2O_5/Al_2O_3 catalysts consist of both isolated and polymeric species [49]. At low surface vanadia coverage (<2 V/nm^2), isolated surface VO_4 species predominated almost exclusively. At monolayer surface vanadia coverage (~8 V/nm^2), the polymeric surface VO_4 species predominated, accounting for almost all of the surface vanadia species. At intermediate vanadium surface density (2–8 V/nm^2), the ratio of polymeric/monomeric surface VO_4 species increased continuously with vanadium surface density. The percentage of polymeric surface VO_4 species with bridging V–O–V bonds in the dehydrated supported vanadia phase also can be quantified from the UV–vis DRS edge energy (E_g) values in the sub-monolayer region, as reported recently by Tian et al. [49].

Fig. 5a illustrates the dependence of the k_{rds} and K_{ads} values on the oxidative dehydrogenation of CH_3OH over the supported V_2O_5/Al_2O_3 catalysts as a function of the percent polymeric vanadium surface density on Al_2O_3. Neither K_{ads}, which reflects the efficiency of breaking the O–H bond of CH_3OH on chemisorption, nor k_{rds}, which reflects the kinetics breaking the of C–H bond of the surface $CH_3O^{\cdot}$ intermediate, depends on the percent polymeric surface VO_4 with bridging V–O–V bonds in the surface vanadium oxide phase. It follows that TOF also does not depend on the percent polymeric surface VO_4 with bridging V–O–V bonds, because TOF depends on the product of $k_{rds}\, K_{ads}$. The constant TOF with increasing vanadium surface density also reflects the participation of only 1 surface VO_4 site in the oxidative dehydrogenation of CH_3OH to HCHO.

Fig. 5b shows the dependence of k_{rds} and K_{ads} on the terminal V=O bond of the surface VO_4 species, with higher wavenumber values corresponding to shorter V=O bonds [61,62]. The V=O vibration of the dehydrated surface VO_4 species shifted to higher cm^{-1} values with increasing vanadium surface density (see Fig. 1). As mentioned earlier, this shift coincided with the extent of polymerization of the surface vanadium oxide species. But the slight shortening of the terminal V=O bond with coverage did not affect the kinetic parameters (k_{rds}, K_{ads}, and TOF) for methanol oxidation over the supported V_2O_5/Al_2O_3 catalysts. Recent theoretical sim-

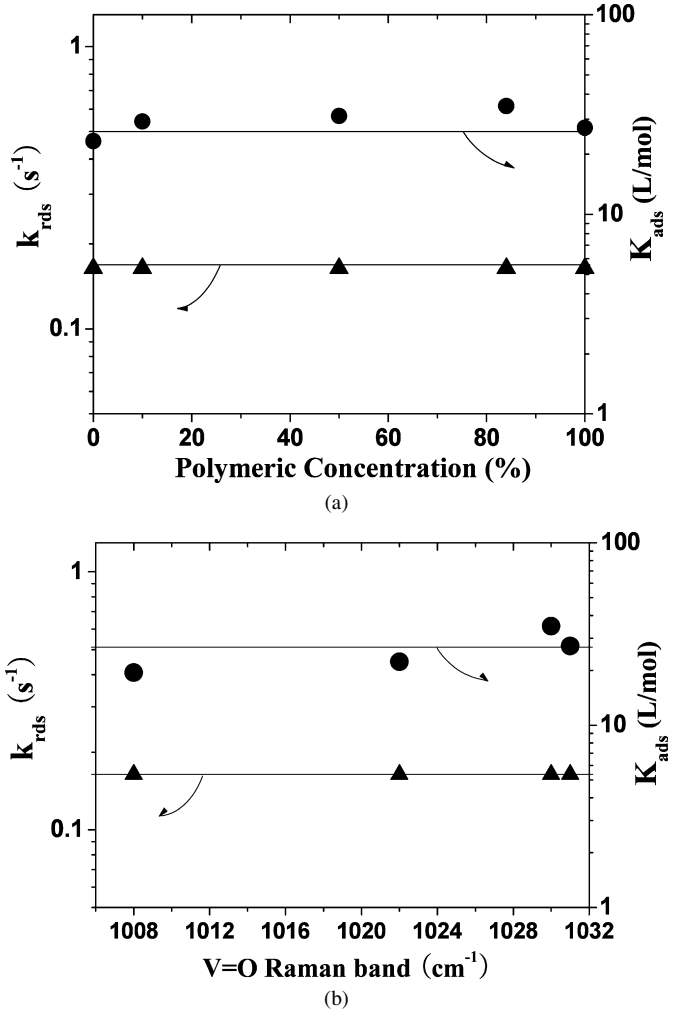

Fig. 5. k_{rds} and K_{ads} values for methanol oxidation over supported V_2O_5/Al_2O_3 catalysts at 230 °C as a function of (a) concentration of polymeric surface VO_4 species and (b) terminal V=O Raman band position.

ulations suggest that the terminal V=O bond is involved in H transfer from the surface methoxy intermediate over isolated surface VO_4 sites (the RDS) [36]. Our findings demonstrate that the minor perturbation of the terminal V=O bond is not sufficiently significant to affect the kinetics of the RDS of C–H bond breaking for the surface $CH_3O^{\cdot}$ intermediate. Furthermore, the terminal V=O bond characteristics also are perturbed in the presence of an H atom.

There is no relationship between the TOF for methanol oxidative dehydrogenation and the nature of surface acid sites or reduction kinetics of the surface VO_4 species during H_2-TPR. It is well established that in the supported V_2O_5/Al_2O_3 catalyst system, the number of surface Brønsted acid sites increases and the number of surface Lewis acid sites remains constant or decreases with vanadium surface density in the sub-monolayer region [24,63,64]. The invariance of the TOF with vanadium surface density suggests that the oxidative dehydrogenation of CH_3OH to HCHO involves only surface redox sites and does not depend on the nature of the surface acid sites. Several studies have found that during H_2-TPR, T_p values either continuously decrease [64–67] or increase [68–74] with increasing vanadium surface density in the sub-monolayer region [65,66,74]. Furthermore, the reduction of the surface V^{5+} to surface V^{3+} occurs in a single reduction stage [74–80]. The constant TOF values for the oxidative dehydrogenation of CH_3OH with vanadium surface density for a given support also demonstrates that probing reduction characteristics with H_2 may lead to erroneous conclusions about the redox characteristics of surface vanadium oxide sites during oxidation reactions, because different bonds are involved in H_2-TPR (H–H) and oxidative dehydrogenation of CH_3OH to HCHO (O–H and C–H).

Table 3 compares the kinetic parameters determined for the oxidative dehydrogenation of CH_3OH to HCHO over supported V_2O_5/Al_2O_3 catalysts from the present study with those from previously reported studies [8,38,52–57]. The TOF values are referenced to the reaction temperature of 230 °C by extrapolating from the different temperatures with an apparent activation energy of 21 kcal/mol, with the normalized TOF values for studies performed at another temperature are given in parentheses [8]. For the steady-state fixed-bed reactor studies, except that of [8], all the methanol oxidation TOF values vary between 0.5 and 1.0×10^{-2} s^{-1} and are within a factor of 2, which may be considered with experimental error. The TOF values reported in [8] are significantly larger ($\sim$4–9 $\times$ 10^{-2} s^{-1}) and related to a factor of 10 mathematical error. The TOF values determined with catalyst wafers in the IR cell are somewhat lower (0.2–0.5 $\times$ 10^{-2} s^{-1}), reflecting the presence of mass transfer limitations in this unconventional reaction cell. The presence

Table 3
Comparison of kinetic parameters for methanol oxidation over supported V_2O_5/Al_2O_3 catalysts from different literature studies

Surface density (V/nm^2)	Reaction temp. (°C)	TOF_{REDOX} $\times 10^2$ (s^{-1})	E_a (kcal/mol)	k_{rds} (s^{-1})	K_{ads} (L/mol)	Reactor types	Ref.
1.1–6.5	230	4–9.3	na	na	na	Fixed bed reactor	[8]
2.7	250	2.2 (1.0)[a]	na	na	na	Fixed bed reactor	[52]
3.5	270	3.4 (0.7)[a]	na	na	na	Fixed bed reactor	[53]
8	230	0.68	na	na	na	Fixed bed reactor	[54]
8	230	0.99	31.8	0.136	54	Fixed bed reactor	[55]
8	230	0.68	na	na	na	Fixed bed reactor	[57]
8	225	0.13 (0.16)[a]	22.5	0.002	6.8×10^3	IR cell reactor	[38]
8	225	0.40 (0.49)[a]	24.8	na	na	IR cell reactor	[56]
7.9	230	0.64	31.7	0.164	27	Fixed bed reactor	Current finding

[a] Extrapolate to 230 °C.

of mass transfer limitations also is reflected in the much lower activation energy values obtained for the IR cell studies (∼22–25 kcal/mol) compared with the steady state fixed-bed reactor findings (∼32 kcal/mol) [38,56]. In addition, the methanol gas phase concentration was only 0.2% in the IR studies (with the low methanol partial pressure necessary to eliminate the gas-phase methanol signals in the IR spectra [38]) and 4–6% in the fixed-bed studies. The mass transfer limitations and the dependence of K_{ads} on the partial pressure of moisture [38] in the IR experiment apparently also affected the k_{rds} and K_{ads} values by almost two orders of magnitude. Thus, care always should be taken when extrapolating kinetic studies from unconventional reactor cells with mass transfer limitations and very different reaction conditions. The kinetic parameters found in the present study are almost identical to the E_a, k_{rds} and K_{ads} values reported for methanol oxidation over supported V_2O_5/Al_2O_3 catalyst in a previous study [55] and reflect the reproducibility of these CH_3OH TPSR and methanol oxidation fixed-bed studies.

5. Conclusions

A series of well-defined supported V_2O_5/Al_2O_3 catalysts consisting of isolated surface VO_4 species at low coverage, polymeric surface VO_4 species at intermediate and high coverage, and crystalline V_2O_5 NPs at above monolayer coverage were successfully synthesized. The kinetic parameters (k_{rds}, K_{ads} and TOF) for CH_3OH oxidation to HCHO over supported V_2O_5/Al_2O_3 were investigated by CH_3OH TPSR and steady-state methanol oxidation studies. Surface VO_4 species were the catalytically active sites; the crystalline V_2O_5 NPs had few exposed catalytically active sites. The selective oxidation of CH_3OH to HCHO was found to involve 1 surface VO_4 site. The first-order rate constant for breaking the C–H bond of the surface $CH_3O^{\cdot}$ species to form HCHO was found to be independent of the surface V–O–V concentration or the concentration of surface VO_4 polymers and also to minor perturbations to the terminal surface V=O bond. In addition, the kinetic parameters for methanol oxidation to formaldehyde over the supported V_2O_5/Al_2O_3 catalysts were also independent of the surface acidity and reducibility, as detected by H_2-TPR.

Acknowledgment

Support from the Department of Energy, Division of Basic Energy Sciences (grant DE-FG 02-93 ER 14350) for this work is gratefully acknowledged.

References

[1] J.M. Miller, L.J. Lakshmi, Appl. Catal. A Gen. 190 (2000) 197.
[2] R.Z. Khaliullin, A.T. Bell, J. Phys. Chem. B 106 (2002) 7832.
[3] S. Irusta, L.M. Cornaglia, I. Miro, E.A. Lombardo, J. Catal. 156 (1995) 167.
[4] G.C. Bond, S.F. Tahir, Appl. Catal. 71 (1991) 1.
[5] J.L. Bronkema, A.T. Bell, J. Phys. Chem. C 111 (2007) 420.
[6] P. Forzatti, E. Tronconi, A.S. Elmi, G. Busca, Appl. Catal. A Gen. 157 (1997) 387.
[7] C.M. Sorensen, R.S. Weber, J. Catal. 142 (1993) 1.
[8] G. Deo, I.E. Wachs, J. Catal. 146 (1994) 323.
[9] J.-M. Jehng, H. Hu, X. Gao, I.E. Wachs, Catal. Today 28 (1996) 335.
[10] G. Deo, I.E. Wachs, J. Catal. 129 (1991) 307.
[11] S.S. Chan, I.E. Wachs, L.L. Murrell, L. Wang, W.K. Hall, J. Phys. Chem. 88 (1984) 5831.
[12] I.E. Wachs, S.S. Chan, R.Y. Saleh, J. Catal. 91 (1985) 366.
[13] G.T. Went, S. Ted Oyama, A.T. Bell, J. Phys. Chem. 94 (1990) 4240.
[14] C. Cristiani, P. Forzatti, G. Busca, J. Catal. 116 (1989) 586.
[15] I.E. Wachs, J. Catal. 124 (1990) 570.
[16] G. Deo, I.E. Wachs, J. Phys. Chem. 95 (1991) 5889.
[17] L.R. Le Coustumer, B. Taouk, M. Le Meur, E. Payen, M. Guelton, J. Grimblot, J. Phys. Chem. 92 (1988) 1230.
[18] J.-M. Jehng, A.M. Turek, I.E. Wachs, Appl. Catal. A Gen. 83 (1992) 179.
[19] R. Kozlowski, R.F. Pettifer, J.M. Thomas, J. Phys. Chem. 87 (1983) 5176.
[20] J. Haber, A. Kozlowska, R.J. Kozlowski, J. Catal. 102 (1986) 52.
[21] H. Eckert, I.E. Wachs, J. Phys. Chem. 91 (1989) 6796.
[22] G. Busca, G. Centi, L. Marchetti, F. Trifiro, Langmuir 2 (1986) 568.
[23] R.B. Brjorklund, C.U.I. Odenbrand, J.G.M. Brandin, L.A.H. Andersson, B. Liedberg, J. Catal. 119 (1989) 187.
[24] A.M. Turek, I.E. Wachs, E. DeCanio, J. Phys. Chem. 96 (1992) 5000.
[25] M.A. Vuurman, I.E. Wachs, A.M. Hirt, J. Phys. Chem. 95 (1991) 9928.
[26] G.C. Bond, J.P. Zurita, S. Flamerz, Appl. Catal. 27 (1986) 353.
[27] Z. Liu, Z. Lin, H. Kan, F. Li, Appl. Phys. A 45 (1988) 159.
[28] X. Gao, S.R. Bare, J.L.G. Fierro, I.E. Wachs, J. Phys. Chem. B 103 (1999) 618.
[29] X. Gao, I.E. Wachs, J. Phys. Chem. B 104 (2000) 1261.
[30] M.A. Banares, M.V. Martinez-Huerta, X. Gao, J.L.G. Fierro, I.E. Wachs, Catal. Today 61 (2000) 295.
[31] A. Khodakov, B. Olthof, A.T. Bell, E. Iglesia, J. Catal. 181 (1999) 205.
[32] G. Busca, J. Mol. Catal. 50 (1989) 241.
[33] C.J. Machiels, W.H. Cheng, U. Chowdhry, W.E. Farneth, F. Hong, E.M. McCarron, A.W. Sleight, Appl. Catal. 25 (1986) 249.
[34] E.M. McCarron, A.W. Sleight, Polyhedron 5 (1986) 129.
[35] M. Calatayud, C. Minot, J. Phys. Chem. C 111 (2007) 6411.
[36] J. Dobler, M. Pritzsche, J. Sauer, J. Am. Chem. Soc. 127 (2005) 10861.
[37] R.S. Weber, J. Phys. Chem. 98 (1994) 2999.
[38] L.J. Burcham, M. Badlani, I.E. Wachs, J. Catal. 203 (2001) 104.
[39] L.J. Burcham, L.E. Briand, I.E. Wachs, Langmuir 17 (2001) 6164.
[40] L.E. Briand, W.E. Farneth, I.E. Wachs, Catal. Today 62 (2000) 219.
[41] T. Feng, J.M. Vohs, J. Catal. 208 (2002) 301.
[42] P.A. Redhead, Vacuum 12 (1962) 213.
[43] I.E. Wachs, T. Kim, E.I. Ross, Catal. Today 116 (2006) 162.
[44] B. Olthof, A. Khodakov, A.T. Bell, E. Iglesia, J. Phys. Chem. B 104 (2000) 1516.
[45] X. Gao, M.A. Banares, I.E. Wachs, J. Catal. 188 (1999) 325.
[46] A. Khodakov, J. Yang, S. Su, E. Iglesia, A.T. Bell, J. Catal. 177 (1998) 343.
[47] M.A. Vuurman, I.E. Wachs, J. Phys. Chem. 96 (1992) 5008.
[48] M.D. Argyle, K. Chen, C. Resini, C. Krebs, A.T. Bell, E. Iglesia, J. Phys. Chem. B 108 (2004) 2345.
[49] H. Tian, E.I. Ross, I.E. Wachs, J. Phys. Chem. B 110 (2006) 9593.
[50] I.E. Wachs, J.-M. Jehng, G. Deo, B.M. Weckhuysen, V.V. Guliants, J.B. Benziger, Catal. Today 32 (1996) 47.
[51] P. Mars, D.W. van Krevelen, Chem. Eng. Sci. Spec. Suppl. 3 (1954) 41.
[52] B. Mitra, I.E. Wachs, G. Deo, J. Catal. 240 (2006) 151.
[53] X. Gao, I.E. Wachs, J. Catal. 192 (2000) 18.
[54] I.E. Wachs, in: J.J. Spivey (Ed.), in: Catalysis, vol. 13, The Royal Society of Chemistry, Cambridge, 1997, pp. 37–54.
[55] X. Wang, I.E. Wachs, Catal. Today 96 (2004) 211.
[56] L.J. Burcham, I.E. Wachs, Catal. Today 49 (1999) 467.
[57] I.E. Wachs, Y. Chen, J.-M. Jehng, L.E. Briand, T. Tanaka, Catal. Today 78 (2003) 13.
[58] W. Holstein, C. Machiels, J. Catal. 162 (1996) 118.
[59] M. Badlani, I.E. Wachs, Catal. Lett. 75 (2001) 137.
[60] L.E. Briand, J.-M. Jehng, L. Cornaglia, A.M. Hirt, I.E. Wachs, Catal. Today 78 (2003) 257.
[61] I.D. Brown, K.K. Wu, Acta Crystallogr. B 32 (1976) 1957.
[62] F.D. Hardcastle, I.E. Wachs, J. Phys. Chem. 95 (1991) 5031.
[63] I.E. Wachs, Catal. Today 27 (1996) 437.

[64] M.V. Martínez-Huerta, X. Gao, H. Tian, I.E. Wachs, J.L.G. Fierro, M.A. Banares, Catal. Today 118 (2006) 279.
[65] F. Klose, T. Wolff, H. Lorenz, A. Seidel-Morgenstern, Y. Suchorski, M. Piorkowska, H. Weiss, J. Catal. 247 (2007) 176.
[66] S. Albonetti, S. Blasioli, A. Bruno, J. Epoupa Mengou, F. Trifiro, Appl. Catal. B Environ. 64 (2006) 1.
[67] P. Concepción, M.T. Navarro, T. Blasco, J.M. Lopez Nieto, B. Panzacchi, F. Rey, Catal. Today 96 (2004) 179.
[68] P.H. Mutin, A.F. Popa, A. Vioux, G. Delahay, B. Coq, Appl. Catal. B Environ. 69 (2006) 49.
[69] A.E. Lewandowska, M.A. Banares, Catal. Today 118 (2006) 323.
[70] I. Giakoumelou, C. Fountzoula, C. Kordulis, S. Boghosian, J. Catal. 239 (2006) 1.
[71] M.I. Kim, D.W. Park, S.W. Park, X. Yang, J.S. Choi, D.J. Suh, Catal. Today 111 (2006) 212.
[72] A. Baiker, P. Dollenmeier, M. Glinski, A. Reller, Appl. Catal. 35 (1987) 351.
[73] R.A. Koepple, J. Nickl, A. Baiker, Catal. Today 20 (1994) 45.
[74] E.V. Kondratenko, M. Cherian, M. Baerns, D. Su, R. Schlögl, X. Wang, I.E. Wachs, J. Catal. 234 (2005) 131.
[75] X. Gao, S.R. Bare, B.M. Weckhuysen, I.E. Wachs, J. Phys. Chem. B 102 (1998) 10842.
[76] M.M. Koranne, J.G. Goodwin, G. Marcelin, J. Catal. 148 (1994) 369.
[77] F. Arena, N. Giordano, A. Parmaliana, J. Catal. 167 (1997) 66.
[78] A. Gervasini, P. Carniti, J. Keranen, L. Niinisto, A. Auroux, Catal. Today 96 (2004) 187.
[79] C. Tellez, M. Abon, J.A. Dalmon, C. Mirodatos, J. Santamaria, J. Catal. 195 (2000) 113.
[80] S. Besselmann, C. Freitag, O. Hinrichsen, M. Muhler, Phys. Chem. Chem. Phys. 3 (2001) 4633.